



Mechanics of Advanced Composite Structures

journal homepage: <http://MACS.journals.semnan.ac.ir>



Tensile and Flexural Properties of 3D-Printed Polylactic Acid/Continuous Carbon Fiber Composite

A. Khalili, A. Kami* , V. Abedini 

Faculty of Mechanical Engineering, Semnan University, Semnan, Iran

KEYWORDS

Additive manufacturing;
Fused deposition modeling;
Polymer matrix composites;
Carbon fiber;
Continuous fiber composites.

ABSTRACT

Fused deposition modeling is one of the most common methods of additive manufacturing that has enabled the 3D printing of composites. Compared with traditional procedures, this method reduces part cost and production time. This paper investigated the effects of layer height, print speed, and nozzle temperature on the tensile and flexural characteristics of polylactic acid/continuous carbon fiber (PLA/CCF) composite. Two predicting models were developed based on the mechanical tests' data to estimate composite specimens' tensile and flexural strength. These models were used in a two-objective optimization procedure to obtain the composite's highest tensile and flexural strength. The optimum layer thickness, print speed, and nozzle temperature values were 0.3 mm, 4 mm/s, and 200°C, respectively. Adjusting the optimal values of the study parameters increased tensile and flexural strength by 77 and 27.5 percent, respectively, over the unreinforced sample. Furthermore, the fracture section of the composite was examined by scanning electron microscopy (SEM). The SEM images showed that the printing parameters influenced fiber impregnation, which in turn affected the sample's strength. Finally, two composite samples were successfully 3D printed with higher complexity using the optimized values of the studied parameters.

1. Introduction

Additive manufacturing (AM) is a new technology that may be used for both production and prototyping. Although AM has made significant development, it is still in its early stages and has flaws compared with traditional manufacturing procedures [1]. Massive research is being carried out to improve and optimize AM methods and product characteristics [2].

Fused deposition modeling (FDM) is a popular extrusion-based AM technique [2]. However, the mechanical qualities of FDM parts are lower than those of plastic injection molded parts [3]. Furthermore, FDM parts are necessary to compete with metallic components in some applications. As a result, efforts were undertaken to improve the mechanical properties of the FDM parts by introducing additives and reinforcements and conducting post-processing [4]. Including either discontinuous or continuous reinforcing fibers is one strategy for improving the characteristics of FDM components [5, 6]. Discontinuous fibers are often included in a polymeric filament, whereas continuous fibers

can be added to the filament or fed independently during 3D printing [7].

Although composites can be made using various traditional methods [8], 3D-printed composites have received a lot of interest in the recent decade because of their tremendous potential for extending their applications from rapid prototyping to end-use products [9]. Continuous fiber-reinforced thermoplastic composites (CFRTCs) have been used in different sectors of industry, such as aerospace, automotive, medical, electronics, and robotics. A variety of components have been made, including wing structures, chassis components of cars, bicycle frames, antennas, and robotic arms [5, 6]. Furthermore, the advancement of AM has opened up new possibilities for the design and manufacture of composites. 3D-printed composites include new materials with distinct features, improved performance, and complicated 3D structures. The various advantages of 3D-printed composites over traditional composites are already well established [10]. Aluminum could be replaced by

* Corresponding author. Tel: +98-23-31532353
Email: akami@semnan.ac.ir

CFRTCs [11]. However, because only a few companies can produce quality 3D printing equipment and materials, the market for FDM CFRTCs has been limited [11]. As a result, significant research is being performed on the 3D printing of CFRTCs to improve their mechanical properties [12].

Apart from the matrix and reinforcement materials, the 3D printing parameters affect the mechanical properties of FDM composites. Each parameter has a distinct influence, and there is some interaction between them. As a result, numerous research has been conducted to investigate this. Kumar et al. [13] carried out impact, tensile, and flexural testing on the PLA/CCF composite. The effects of layer thickness, raster angle, infill density, and printing speed were studied. The results showed that printing speed had the most significant effect on tensile strength, but raster angle and layer thickness had the most influence on flexural and impact strength, respectively. Carneiro et al. [14] studied FDM 3D printing of polypropylene (PP) and PP/30 wt.% glass fibers composites. They discovered glass fibers increased tensile strength by about 40%. Dickson et al. [15] investigated the properties of nylon matrix composites reinforced with carbon, Kevlar, and glass fibers. They looked at how fiber orientation and fiber volume fraction affected tensile and flexural characteristics. The mechanical strength of nylon/carbon fiber composites was the highest, followed by glass fiber and Kevlar fiber-reinforced composites. Furthermore, the tensile and flexural strength of the nylon/carbon fiber composite was 6.3 and 5 times higher, respectively, than plain nylon. Jiang and Smith [16] performed tensile experiments on 3D-printed pure and carbon fiber-reinforced PLA, ABS, PETG, and Amphora. They concluded that the tensile strength of all carbon-fiber-reinforced specimens with a zero-degree print direction was significantly greater than that of non-reinforced specimens. However, when printed with beads not aligned with the loading direction, the addition of carbon fiber decreased tensile strength for some materials. Melenka et al. [17] evaluated the tensile characteristics of nylon/Kevlar fiber composites with fiber volume percentages of 4.04, 8.08, and 10.1. The composites' tensile moduli were 1767.2 MPa, 6920 MPa, and 9001.2 MPa, respectively. Goh et al. [18] looked at the tensile, flexural, and quasi-static indentation properties of carbon and glass fiber-reinforced composites. Carbon fiber-reinforced composites performed better in tensile and flexural testing. Naranjo-Lozada et al. [19] studied the effect of infill percentage, infill pattern, fiber volume percentage, and printing geometry on continuous and discontinuous carbon fiber-reinforced composites. They

concluded that the triangular infill design outperforms the rectangular pattern in tensile performance. Furthermore, the tensile property of the composite samples was improved by increasing the volume percentage of continuous fibers. Bettini et al. [20] looked into the tensile and compressive characteristics of a PLA/aramid fiber composite. In addition, they 3D printed glass and carbon fiber-reinforced composites. However, the 3D printing of PLA/carbon fiber and PLA/glass fiber composites was not successful due to the failure of the glass and carbon fibers. The tensile strength and modulus of the PLA/aramid fiber composite were approximately 6 and 3 times those of pure PLA, respectively. Van De Werken et al. [21] studied the mechanical characteristics of composites made of nylon and carbon fibers. Finite element analysis was also employed to explain composite sample failure better. It was also discovered that the geometry, infill pattern, and infill percentage substantially impacted the mechanical properties. Li et al. [22] pre-impregnated carbon fiber using a methylene chloride solution containing 8% PLA. The tensile and flexural strength of composites manufactured from pre-impregnated fibers increased by approximately 13.8% and 164%, respectively. Luo et al. [23] 3D printed polyetheretherketone (PEEK)/carbon fiber composites with pre-impregnation and in-situ laser heating. Using this approach, the composite's interlayer shear and flexural strength enhanced to more than 35 MPa and 480 MPa, respectively. Tian et al. [24] investigated how printing temperature, layer height, filament feed rate, overlap, and print speed affected the flexural characteristics of PLA/carbon fiber composites. They achieved flexural strength and modulus of 335 MPa and 30 GPa, respectively, by optimizing these characteristics. The mechanical properties of PLA/CCF composites produced in a vacuum chamber were examined by Li et al. [25]. The findings revealed that negative pressure increases composite layer bonding and decreases cavities (4.18%). As a result, printing samples in the vacuum chamber increased flexural strength and modulus by 24.51% and 8.35%, respectively. Furthermore, the results demonstrated flexural characteristics are strongly connected to printing temperature and inversely related to printing speed and layer height. Araya-Calvo et al. [26] investigated the impact of various process factors on the compressive and flexural characteristics of PA6/CCF composites. The maximum compressive and flexural stresses were 53.3 MPa and 231.1 MPa, respectively, with fiber volume percentages of 24.44 and 48.93. Yang et al. [27] 3D printed ABS/CCF composites concurrently impregnating the continuous fiber with ABS. As a result, they created composites with tensile and

flexural strengths of 147 MPa and 127 MPa, respectively.

Despite substantial research on 3D printing continuous fiber composites, additional research is needed to optimize the conditions for 3D printing of composites by making minor modifications to ordinary FDM 3D printers. This study examined the parameters influencing the tensile and flexural properties of a 3D-printed PLA/carbon fiber composite. A dual-nozzle desktop FDM printer originally designed for polymer printing was slightly changed to manufacture CCF composites. The current work contributes by evaluating the tensile and flexural properties concurrently. Additionally, the reinforced layers' number, geometry, and structure differ from earlier investigations. The tensile and flexural strengths were defined as the fitness functions of a multi-objective optimization procedure. The optimal layer thickness, print speed, and nozzle temperature values resulted in the highest tensile and flexural strength.

2. Materials and Methods

The CFRTC is constructed with Y&S PLA filament (Guangzhou, China) and T300-1K continuous carbon fiber (Teijin, Japan). A Sizan4 dual-extruder machine (Sizan Pardazesh Kavir, Iran) was used to 3D print the composite. This desktop FDM printer (see Fig. 1) was initially

designed for polymer printing. However, it was slightly modified to manufacture CFRTC. One nozzle was used to deposit pure PLA, and the other to deposit PLA/CCF. The nozzle had a 1 mm diameter opening. For inserting the carbon fiber, a 0.3 mm diameter slanted hole was drilled in the body of the brass nozzle, as illustrated in Fig. 1. Figure 2 depicts an overview of the 3D printing process.

Only a few layers are reinforced to produce cost-effective components, and the rest layers are 3D printed with a pure polymer (or maybe with less carbon fiber content). Furthermore, carbon fiber-containing layers typically have a poor appearance when compared to pure polymer layers. Given these facts, the composite samples were 3D printed in the form illustrated in Fig. 3 to generate samples with high strength and a smooth surface.

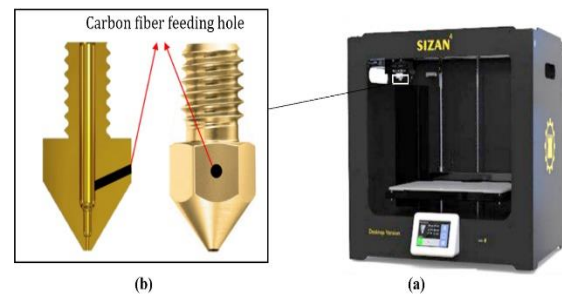


Fig. 1. (a) Sizan4 dual-extruder machine, (b) the nozzle used for feeding carbon fiber with a slanted hole of 0.3 mm diameter

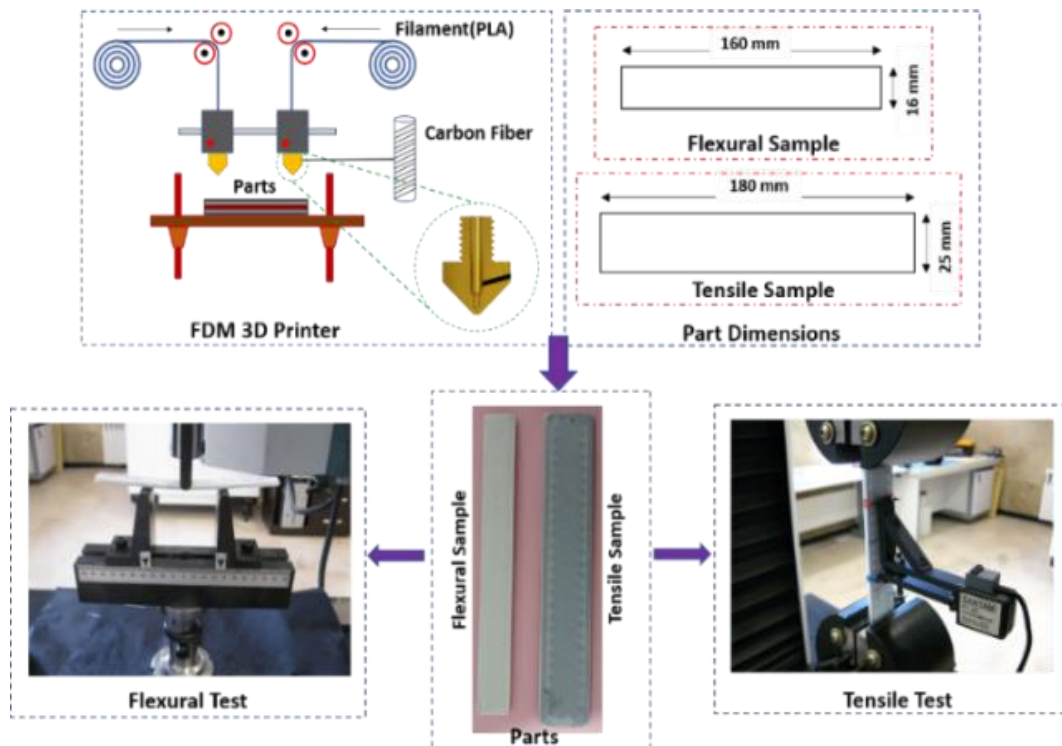


Fig. 2. Schematic illustration of the PLA/carbon fiber composite 3D printing, dimensions of the tensile and flexural test samples, and the experimental setup of the tests

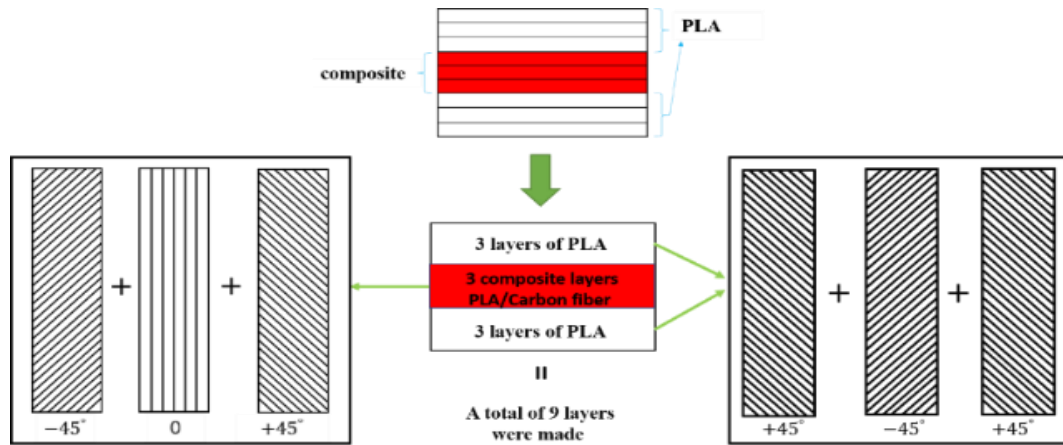


Fig. 3. Structure of the 3D-printed PLA/CCF composite and the raster angle at each layer

The bottom three layers were entirely constructed of PLA. The carbon fiber was then incorporated into the second nozzle, and three layers of PLA/CCF composite were created. The remaining three layers on top of the samples were also made of pure PLA. The raster angles for each layer are shown in Fig. 3. These values were identical in all samples. Furthermore, the PLA layer's infill percentage, PLA/CCF composite layer's infill percentage, deposition overlap, and bed temperature were configured to the values shown in Table 1.

Tensile and flexural tests were carried out following ASTM D3039 [28] and ASTM D790 [29] standards. The experiments were conducted on an STM-50 universal testing machine (SANTAM co., Iran) with a capacity of 50 kN. The tensile test speed was set to 2 mm/min, and the flexural test speed was computed using Eq. (1):

$$R = 0.01L^2/6d \quad (1)$$

where R , L , and d are the bending speed, bending span, and sample thickness, respectively.

Three parameters were investigated: layer height, print speed, and nozzle temperature. These factors were evaluated in the 0.3 – 0.5 mm, 4 – 12 mm/s, and 200 – 230 °C ranges, respectively (see Table 2). The tests were designed using a central composite design (CCD) response surface methodology (RSM). Design-Expert ® 12 software was used to create the experiments. The described approach yielded 17 experiments, which are listed in Table 3. Tensile and flexural tests were carried out by the values stated in each row of Table 3.

3. Result and Discussion

3.1. Results of Tensile and Flexural Tests

Tensile and flexural loads were applied to the samples in Table 3.

Table 1. Parameters that are kept unchanged during 3D printing

PLA layer's infill percentage	PLA/CCF composite layers infill percentage	Deposition overlap (%)	Bed temperature (°C)
100	60	30	60

Table 2. The studied parameters and their values in the CCD

Levels	Layer's thickness (mm)	Print speed (mm/s)	Print temperature (°C)
1	0.3	4	200
2	0.4	8	215
3	0.5	12	230

Table 3. Recommended values of test design software for selected parameters

Test No.	Layer's thickness (mm)	Print speed (mm/s)	Print temperature (°C)
1	0.3	4	200
2	0.5	4	200
3	0.3	12	200
4	0.5	12	200
5	0.3	4	230
6	0.5	4	230
7	0.3	12	230
8	0.5	12	230
9	0.3	8	215
10	0.5	8	215
11	0.4	4	215
12	0.4	12	215
13	0.4	8	200
14	0.4	8	230
15	0.4	8	215
16	0.4	8	215
17	0.4	8	215

In this table, samples #15, #16, and #17 are the center points of the CCD; their results are used to ensure the repeatability of the experiments.

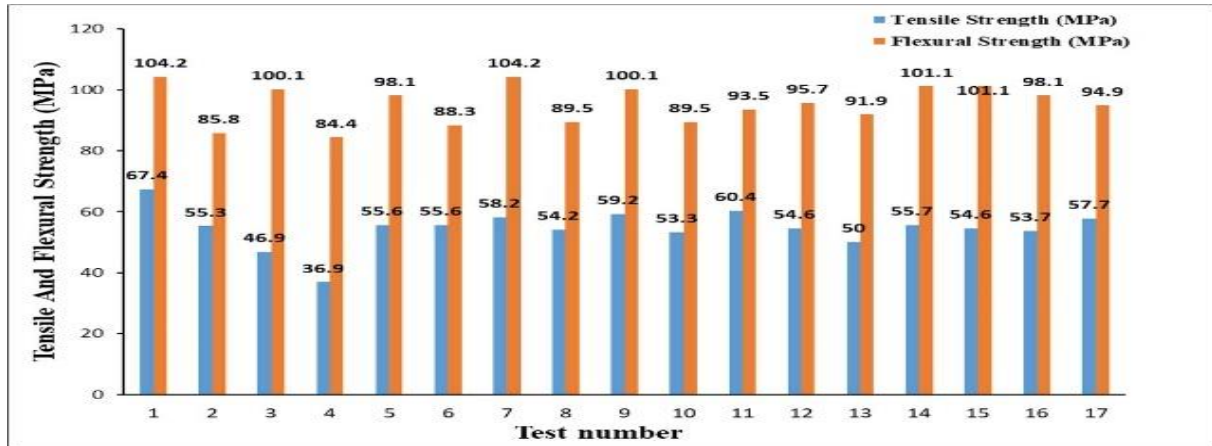


Fig. 4. Tensile and flexural strengths of the designed experiments

Figure 4 depicts the tensile and flexural test results. According to this figure, the center points have tensile strengths of 54.6, 53.7, and 57.7 MPa (with a standard deviation of 2.1 MPa), and flexural strengths of 101.1, 98.1, and 94.9 MPa (with a standard deviation of 3.1 MPa). Therefore, it may be said that the experiments are trustworthy. Some samples after these tests are illustrated in Fig. 5.

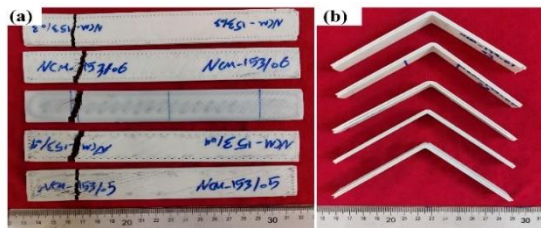


Fig. 5. (a) Tensile and (b) flexural samples after the test

3.2. ANOVA Results for Tensile Strength

Using the data presented in Table 3 and Fig. 4, interpolating models that best approximated the test samples' tensile and flexural strengths were chosen. The power function shown in Eq. (2) was obtained for the prediction of the tensile strength:

$$\begin{aligned}
 & (Tensile\ strength)^{-0.33} \\
 & = 0.2646 + 0.0055 * (A) \\
 & + 0.0043 * (B) - 0.0049 \\
 & * (C) + 0.0016 * (AB) \\
 & - 0.0042 * (AC) \\
 & - 0.0089 * (BC) \\
 & + 0.0054 * (C^2) \\
 & + 0.0042 * (A^2 * B)
 \end{aligned} \tag{2}$$

where *A*, *B*, and *C* are the layer's thickness, printing speed, and printing temperature, respectively.

The Analysis of Variance (ANOVA) was used to determine the extent of the studied parameters' effect and their statistical significance. Table 4 presents the results of ANOVA for the tensile tests' strength. In this table, the p-values less than 0.05 reflect the significance of each term—furthermore, the greater the f-value, the more significant each term's impact. As a result, the interaction between print speed and print temperature (i.e., *BC*) had the most significant impact on tensile strength. The second and third positions are assigned to *A* (layer thickness) and *C* (print temperature), respectively.

Table 4. ANOVA results for the tensile strength

Source	Sum of Squares	df	Mean Square	F-value	p-value	
Model	0.0021	8	0.0003	56.14	< 0.0001	significant
A - Layer's thickness	0.0003	1	0.0003	66.63	< 0.0001	
B - Print speed	0	1	0	8.08	0.0218	
C - Print temperature	0.0002	1	0.0002	52.64	< 0.0001	
AB	0	1	0	4.20	0.0746	
AC	0.0001	1	0.0001	30.67	0.0005	
BC	0.0006	1	0.0006	136.76	< 0.0001	
C ²	0.0001	1	0.0001	25.70	0.0010	
A ² B	0	1	0	5.99	0.0401	
Residual	0	8	4.60E-06			
Lack of Fit	0	6	2.50E-06	0.23	0.9325	not significant

Table 5 displays the coefficient of determination (R^2), adjusted R^2 , and predicted R^2 values for the interpolation function of the tensile strength (i.e., Eq. (2)). All these statistics have values close to one. Furthermore, the adequate precision of 34.684 shows that Eq. (2) is highly accurate. Thus, one may conclude that Eq. (2) can make reliable tensile strength predictions.

Table 5. Statistical values of the model predicted for the tensile test

R^2	Adjusted R^2	Predicted R^2	Adequate Precision
0.983	0.965	0.947	34.684

The perturbation plot in Fig. 6 depicts the change in tensile strength as a function of the parameter values. In this figure, the associated parameter varies between [-1, 1] for each curve, while the others remain constant at the center point (coded value of zero). The steeper the slope of each curve, the greater the effect of the parameter on the tensile strength. As illustrated in Fig. 6, the layer's thickness and print speed have comparable slopes and thus have comparable effects on tensile strength.

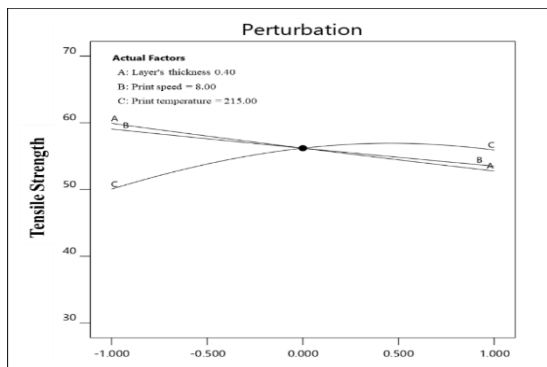


Fig. 6. Perturbation plot showing the relative significance of the studied parameters on the tensile strength

Tensile strength diminishes as the layer's thickness and print speed are increased. Increases in the print temperature up to 215°C (the center point) improve tensile strength, but further increases have no discernible effect.

Figure 7(A) depicts a surface plot for the interaction between layer thickness and print speed, with tensile strength as the output. According to this diagram, there is no interaction between the layer thickness and print speed. Overall, the best tensile strength is obtained when the layer thickness and print speed are set to their smallest values (0.3 mm and 4 mm/s, respectively). The reason for this observation is that layer adhesion rises as layer thickness decreases. Slowing down the printing speed, on the other hand, promotes the impregnation of the

fibers, which aids in the bonding of the fibers to the matrix. Reduced printing speed also reduces fiber tension in the corners, resulting in a more uniform distribution of fibers in the sample and a larger percentage of fibers. Figure 7(B) illustrates a surface plot of tensile strength versus print temperature and layer thickness. Based on this plot, one may conclude that the interaction between these parameters is insignificant.

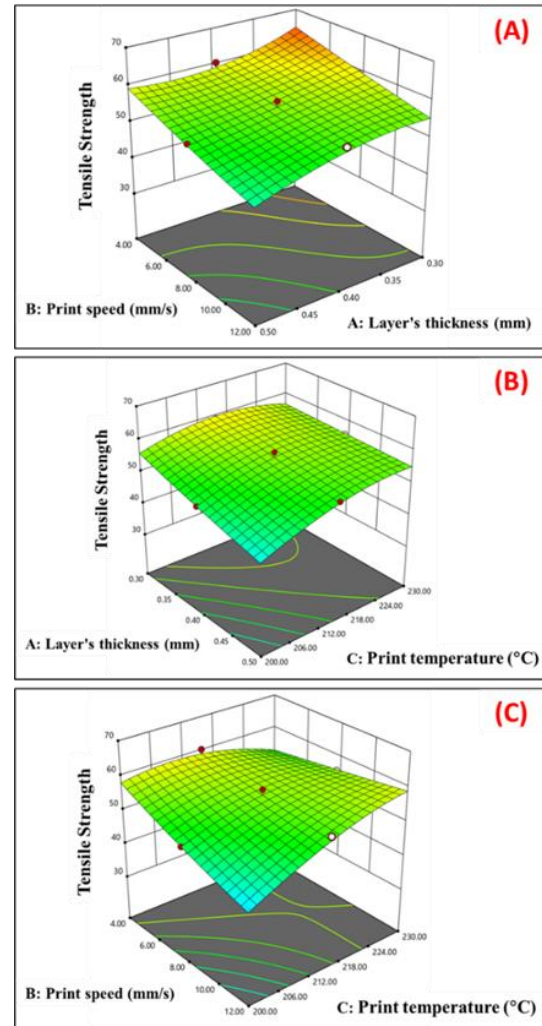


Fig. 7. Surface plots of the interaction between the printing parameters considering the tensile strength as the output; interactions of (A) layer thickness and print speed, (B) layer thickness and print temperature, and (C) print speed and print temperature

The impregnation of the carbon fiber with the molten filament is minimal at low temperatures. As a result, as the printing temperature drops, so does the tensile strength. Figure 7(C) shows the surface plot of tensile strength against print speed and print temperature. According to this plot, the tensile strength improves with decreasing print temperature at the lowest print speed and falls with decreasing print temperature at the maximum print speed. It can be seen that high speed creates fiber tension in

the corners, resulting in decreased fiber volume in the sample. Furthermore, lowering the temperature minimizes fiber impregnation. The tensile strength has grown with decreasing speed at the lowest temperature because fibers' impregnation and layer adhesion are weak at low temperatures. At maximum temperatures, the strength falls as the print speed drops because slowing down allows the matrix to cool and reduces adhesion.

3.3. ANOVA Results for Flexural Strength

Table 6 displays the ANOVA results for the flexural test data. According to this table, the interpolation model is meaningful because its p-value is less than 0.05. ANOVA indicates that A (layer thickness) has the most significant effect on flexural strength. The impact of the other parameters on the flexural strength is negligible compared to A.

Equation (3) displays the interpolation model for flexural strength in terms of the coded values for the parameters.

The coefficient of determination (R^2), modified R^2 , and anticipated R^2 values for this equation are shown in Table 7. These values confirm the model's accuracy. The effect of layer thickness, print speed, and print temperature on flexural strength was evaluated according to the experimental design (Table 3).

Figure 8 displays the influence of each parameter on flexural strength. None of the parameters in this figure have a linear

relationship with the flexural strength of the PLA/FCC composite. Flexural strength decreases significantly as layer thickness increases. Additionally, the print temperature affects flexural strength inversely. As the print temperature grows, the flexural strength increases. Variations in print speed have a negligible effect on flexural strength. Fig. 9(A) shows the flexural strength response surface graph with layer thickness and print temperature. The print speed was set to 8 m/s (the mid-level). This graph shows that print temperature has a negligible effect compared to layer thickness. Flexural strength rises dramatically as layer thickness is decreased at any print temperature. As shown in Fig. 9(A), the maximum flexural strength is obtained when the layer thickness and print temperature are at their minimum values (0.3 mm and 200 °C, respectively).

$$\begin{aligned}
 & (\text{Flexural strength})^{-3} \\
 & = (1.096e - 6) \\
 & + (2.671e - 7) * (A) \\
 & - (1.256e - 8) * (B) \\
 & - (1.602e - 7) * (C) \\
 & - (5.769e - 8) * (AC) \\
 & - (5.339e - 8) * (BC) \\
 & + (8.087e - 8) * (A^2) \\
 & + (6.639e - 8) * (B^2) \\
 & + (1.185e - 7) * (A^2C)
 \end{aligned} \tag{3}$$

Table 6. ANOVA results for the flexural strength

Source	Sum of Squares	df	Mean Square	F-value	p-value	
Model	8.973E-13	8	1.12E-13	20.39	0.0001	significant
A - Layer's thickness	7.132E-13	1	7.13E-13	129.65	< 0.0001	
B - Print speed	1.577E-15	1	1.58E-15	0.2866	0.6070	
C - Print temperature	5.13E-14	1	5.13E-14	9.33	0.0157	
AC	2.662E-14	1	2.66E-14	4.84	0.0590	
BC	2.28E-14	1	2.28E-14	4.14	0.0762	
A ²	1.98E-14	1	1.98E-14	3.60	0.0943	
B ²	1.335E-14	1	1.34E-14	2.43	0.1579	
A ² C	2.246E-14	1	2.25E-14	4.08	0.0780	
Residual	4.401E-14	8	5.50E-15			
Lack of Fit	2.353E-14	6	3.92E-15	0.38	0.8471	not significant

Table 7. Statistical values of the model predicted for the flexural test

R^2	Adjusted R^2	Predicted R^2	Adequate Precision
0.983	0.965	0.947	34.684

As the layer thickness is reduced, the flexural strength of the structure is increased (see Fig. 8 and Fig. 9(A)). This observation is due to increased layer adhesion. Contrary to predictions, the maximum flexural strength was seen at the print's lowest temperature level.

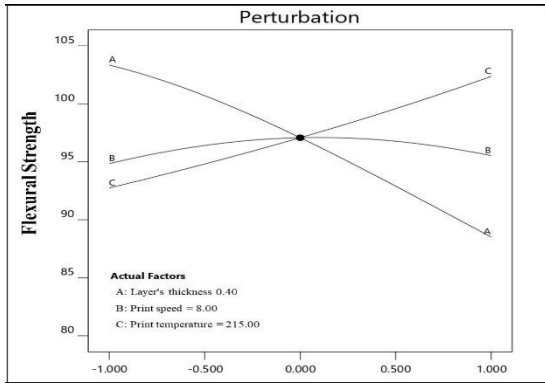


Fig. 8. Perturbation plot showing the relative significance of the studied parameters on the flexural strength

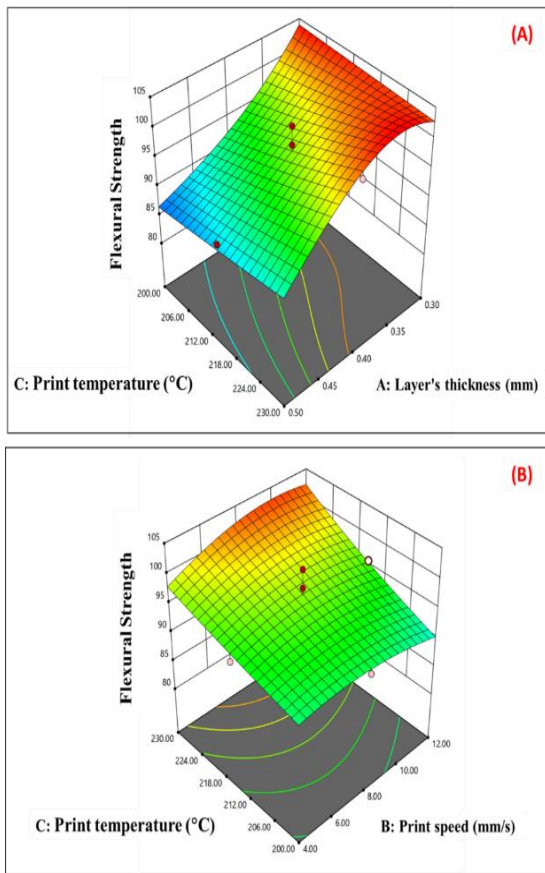


Fig. 9. Surface plots of the interaction between the printing parameters considering the flexural strength as the output; interactions of (A) layer thickness and print temperature, and (B) print speed and print temperature

While the adhesion of the layers increases as the print temperature increases, the matrix's viscoelastic characteristics increase as well, pulling the fibers into the corners and reducing the percentage of fibers in the sample. The response surface plot of the flexural strength with print speed and temperature is shown in Figure 9(B). According to this figure, the flexural strength increases as the print temperature increases, owing to increased layer adhesion. Additionally, raising the print speed stops the bottom layers from rapidly cooling, resulting in a stronger sample.

3.4. Multi-objective Optimization of Parameters

A multi-objective optimization procedure was used to determine the printing condition that results in maximum tensile and flexural strength. The parameters under investigation varied within the ranges provided in Table 2. The optimization was carried out using the fitness functions defined in Eqs. (2) and (3), which specified the tensile and flexural strengths, respectively. Tensile and flexural strengths were limited to 67.41 MPa and 104.22 MPa, respectively (see Fig. 4). The optimization results are shown in Table 8. According to this table, the maximum tensile and flexural strengths were 67.23 MPa and 102.83 MPa, respectively. These values correspond to the layer thickness of 0.3 mm, print speed of 4 mm/s, and print temperature of 200°C. As stated in Table 3, these values correspond to sample #1, which possesses the highest tensile and flexural strengths (see Fig. 4). As a result, the fitness functions and optimization process are both trustworthy.

Screening experiments were done to investigate the effect of fiber reinforcement. On the other hand, fiber-free (pure PLA) and fiber-reinforced (PLA/CCF) samples were printed and then subjected to tensile and flexural tests. The printing condition was set to the optimized values (see Table 8). As illustrated in Fig. 10, the addition of carbon fibers raised the tensile and flexural strengths by 77% and 27.5%, respectively.

Table 8. The optimal values of the parameters and the predicted maximum tensile and flexural strength

Factor	Layer thickness (mm)	Print speed (mm/s)	Print temperature (°C)	Tensile strength (MPa)	Flexural Strength (MPa)	Desirability
Value	0.3	4	200	67.23	102.83	0.974

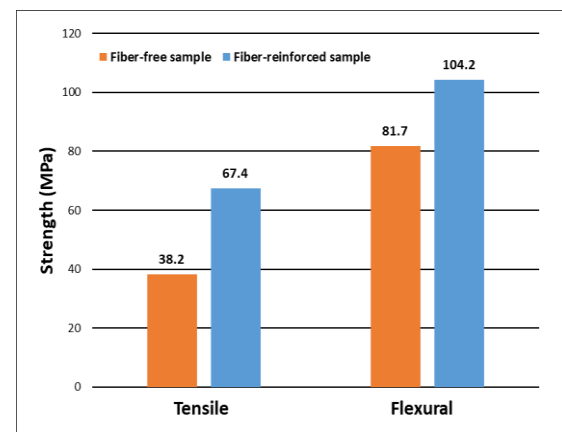


Fig. 10. Tensile and flexural strength values of fiber-reinforced and fiber-free (PLA) specimens

Two components with complicated geometries were produced by adjusting the optimal parameters (see Fig. 11). The goal was to assess the applicability of the FDM print setup and the reliability of the optimization technique for more realistic industrial components. These components were successfully printed and had an acceptable quality. As a result, one could conclude that the printing setup is suitable for industrial purposes, and the proposed optimization process and its output generated trustworthy findings.



Fig. 11. Parts produced with complex geometries

3.5. Scanning Electron Microscopy of Fracture Sections

The fracture surface was examined using scanning electron microscopy (SEM). Two samples were selected for SEM analysis: samples #1 and #4, which had the highest and lowest mechanical properties (tensile and flexural strengths), respectively.

Figures 12 and 13 show SEM images of the fracture surfaces of these samples. Fiber impregnation is a critical factor in the adherence of fibers and matrix, increasing the part's ultimate strength. Before printing, the fibers were not impregnated, and it was intended to accomplish during printing. According to Fig. 13, sample #1 has a higher impregnation than sample #4, resulting in increased tensile and flexural strengths. Thus, one can deduce that by changing the printing condition, one can improve the impregnation of the fibers and thus their mechanical qualities.

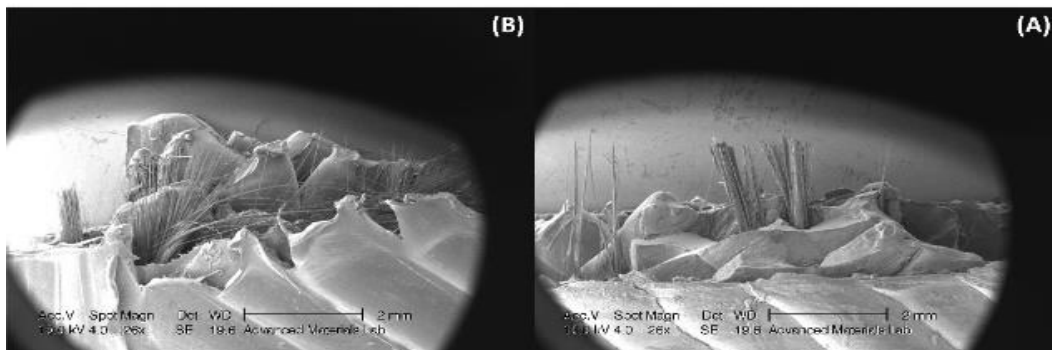


Fig. 12. SEM images of the fractured surfaces of (A) sample #1 and (B) sample #4

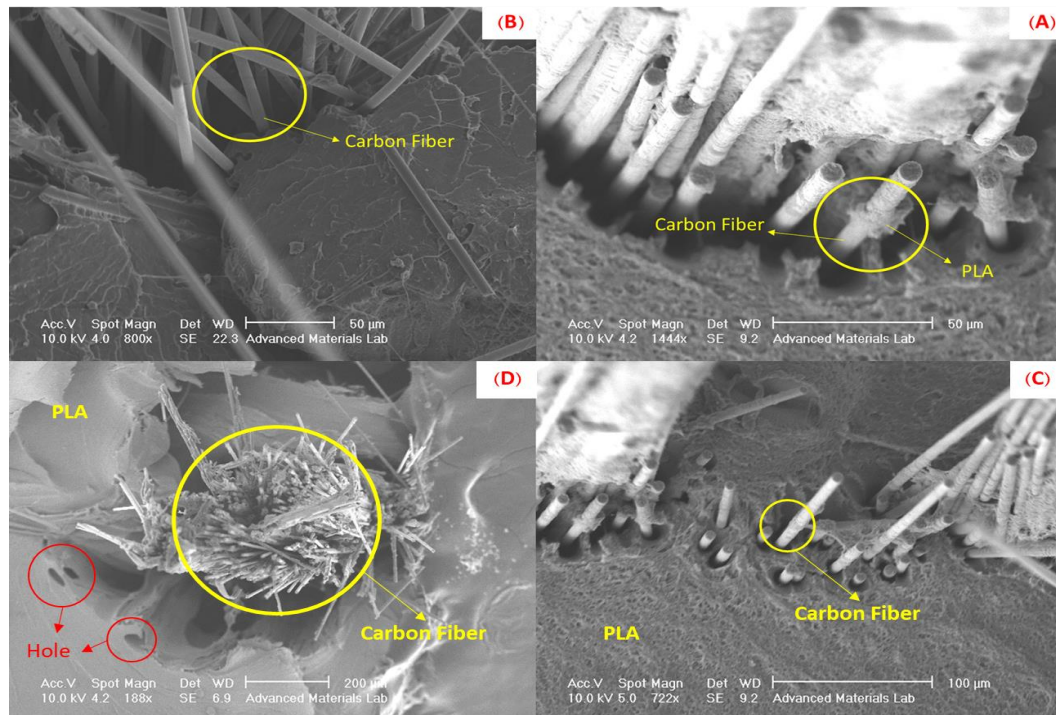


Fig. 13. SEM image representing the fiber impregnation for (A, C) sample #1 (B, D) sample #4

However, successful impregnation depends on the print setup. Because of the limited interaction between fibers and molten PLA, obtaining perfect impregnation was unachievable with the setup used in this work. Furthermore, Fig. 13 shows some holes near the fibers, which may develop because of the fibers' pulling. In sample #4, PLA did not penetrate the carbon fibers. This phenomenon had a detrimental effect on the mechanical performance of sample #4.

Generally, polymers exhibit brittle failure mechanisms caused by micro-cracking. They fail over a longer period and are under less stress. While ductile fractures entail significant plastic deformation, brittle fractures involve little to no macroscopically clear plastic deformation. Brittle fractures in polymers happen at small strains without considerable plastic deformation [30]. According to Fig. 13, the matrix's (PLA's) fracture section is smooth and contains visible cleavage facets, showing brittle fracture. The cleavage facets result from brittle fracture along with flat-faced crystallographic plates.

4. Conclusions

This study employed the FDM technique to 3D print a PLA/CCF composite. The optimal conditions for creating high-strength parts were determined by analyzing the parameters affecting the mechanical properties of this composite. An experimental design and multi-objective optimization accomplished this goal. The most significant findings from this study are:

The method chosen to print PLA/CCF composites produced satisfactory results. Additionally, printing conditions affect the impregnation of the fibers and, hence, the composite's mechanical properties. The tensile strength of composite specimens generally increases as the temperature and print speed parameters are decreased. It was found that the layer height and print speed had the most significant and minor influence on flexural strength, respectively. The sample with a layer height of 0.3 mm, a print speed of 4 mm/s, and a nozzle temperature of 200°C exhibited the best tensile and flexural strength. Compared to unreinforced samples (pure PLA), the PLA/CCF composite sample produced under optimum printing conditions exhibited approximately 77% and 27.5% greater tensile and flexural strengths, respectively. SEM images of the composite samples' fracture sections revealed that fiber impregnation affected the mechanical properties. As a result, it is critical to optimize impregnation to generate high-strength composites. The results indicated it is possible to have some control over the impregnation by altering the printing conditions.

Conflicts of Interest

The authors have no conflicts of interest to declare relevant to this article's content.

References

- [1] Arif, Z.U., Khalid, M.Y., Al Rashid, A., Ur Rehman, E. & Atif, M., 2022. Laser deposition of high-entropy alloys: A comprehensive review. *Optics & Laser Technology*, 145, pp.107447.
- [2] Arif, Z.U., Khalid, M.Y. & Rehman, E.U., 2022. Laser-aided additive manufacturing of high entropy alloys: Processes, properties, and emerging applications. *Journal of Manufacturing Processes*, 78, pp.131-171.
- [3] Behalek, L., Safka, J., Seidl, M., Habr, J. & Bobek, J., 2018. Fused deposition modelling vs. Injection moulding: Influence of fiber orientation and layer thickness on the mechanical properties. *MM Sci. J*, 2018, pp.2722-2726.
- [4] Khalid, M.Y., Arif, Z.U. & Ahmed, W., 2022. 4d printing: Technological and manufacturing renaissance. 307 (8), pp.2200003.
- [5] Kabir, S.F., Mathur, K. & Seyam, A.-F.M., 2020. A critical review on 3d printed continuous fiber-reinforced composites: History, mechanism, materials and properties. *Composite Structures*, 232, pp.111476.
- [6] Safari, F., Kami, A. & Abedini, V., 2022. 3d printing of continuous fiber reinforced composites: A review of the processing, pre- and post-processing effects on mechanical properties. *Polymers and Polymer Composites*, 30.
- [7] Dey, A., Roan Eagle, I.N. & Yodo, N., 2021. A review on filament materials for fused filament fabrication. *Journal of manufacturing and materials processing*, 5 (3), pp.69.
- [8] Bagheri, S., Kami, A. & Shakouri, M., 2022. Single point incremental forming of polyamide/30 wt% short glass fiber composite. *Journal of Thermoplastic Composite Materials*, pp.08927057221083497.
- [9] Arif, Z.U., Khalid, M.Y., Noroozi, R., Sadeghianmaryan, A., Jalalvand, M. & Hossain, M., 2022. Recent advances in 3d-printed polylactide and polycaprolactone-based biomaterials for tissue engineering applications. *International Journal of*

- Biological Macromolecules*, 218, pp.930-968.
- [10] Yuan, S., Li, S., Zhu, J. & Tang, Y., 2021. Additive manufacturing of polymeric composites from material processing to structural design. *Composites Part B: Engineering*, 219, pp.108903.
- [11] Zhuo, P., Li, S., Ashcroft, I.A. & Jones, A.I., 2021. Material extrusion additive manufacturing of continuous fibre reinforced polymer matrix composites: A review and outlook. *Composites Part B: Engineering*, 224, pp.109143.
- [12] Harris, M., Potgieter, J., Archer, R. & Arif, K.M., 2019. Effect of material and process specific factors on the strength of printed parts in fused filament fabrication: A review of recent developments. *Materials*, 12 (10), pp.1664.
- [13] Kumar, K.R., Mohanavel, V. & Kiran, K., 2022. Mechanical properties and characterization of polylactic acid/carbon fiber composite fabricated by fused deposition modeling. *Journal of Materials Engineering and Performance*, pp.1-10.
- [14] Carneiro, O.S., Silva, A. & Gomes, R., 2015. Fused deposition modeling with polypropylene. *Materials & Design*, 83, pp.768-776.
- [15] Dickson, A.N., Barry, J.N., McDonnell, K.A. & Dowling, D.P., 2017. Fabrication of continuous carbon, glass and kevlar fibre reinforced polymer composites using additive manufacturing. *Additive Manufacturing*, 16, pp.146-152.
- [16] Jiang, D. & Smith, D.E., 2017. Anisotropic mechanical properties of oriented carbon fiber filled polymer composites produced with fused filament fabrication. *Additive Manufacturing*, 18, pp.84-94.
- [17] Melenka, G.W., Cheung, B.K.O., Schofield, J.S., Dawson, M.R. & Carey, J.P., 2016. Evaluation and prediction of the tensile properties of continuous fiber-reinforced 3d printed structures. *Composite Structures*, 153, pp.866-875.
- [18] Goh, G.D., Dikshit, V., Nagalingam, A.P., Goh, G.L., Agarwala, S., Sing, S.L., Wei, J. & Yeong, W.Y., 2018. Characterization of mechanical properties and fracture mode of additively manufactured carbon fiber and glass fiber reinforced thermoplastics. *Materials & Design*, 137, pp.79-89.
- [19] Naranjo-Lozada, J., Ahuett-Garza, H., Orta-Castañón, P., Verbeeten, W.M. & Sáiz-González, D., 2019. Tensile properties and failure behavior of chopped and continuous carbon fiber composites produced by additive manufacturing. *Additive Manufacturing*, 26, pp.227-241.
- [20] Bettini, P., Alitta, G., Sala, G. & Di Landro, L., 2017. Fused deposition technique for continuous fiber reinforced thermoplastic. *Journal of Materials Engineering and Performance*, 26 (2), pp.843-848.
- [21] Van De Werken, N., Hurley, J., Khanbolouki, P., Sarvestani, A.N., Tamijani, A.Y. & Tehrani, M., 2019. Design considerations and modeling of fiber reinforced 3d printed parts. *Composites Part B: Engineering*, 160, pp.684-692.
- [22] Li, N., Li, Y. & Liu, S., 2016. Rapid prototyping of continuous carbon fiber reinforced polylactic acid composites by 3d printing. *Journal of Materials Processing Technology*, 238, pp.218-225.
- [23] Luo, M., Tian, X., Shang, J., Zhu, W., Li, D. & Qin, Y., 2019. Impregnation and interlayer bonding behaviours of 3d-printed continuous carbon-fiber-reinforced poly-ether-ether-ketone composites. *Composites Part A: Applied Science and Manufacturing*, 121, pp.130-138.
- [24] Tian, X., Liu, T., Yang, C., Wang, Q. & Li, D., 2016. Interface and performance of 3d printed continuous carbon fiber reinforced pla composites. *Composites Part A: Applied Science and Manufacturing*, 88, pp.198-205.
- [25] Li, H., Liu, B., Ge, L., Chen, Y., Zheng, H. & Fang, D., 2021. Mechanical performances of continuous carbon fiber reinforced pla composites printed in vacuum. *Composites Part B: Engineering*, 225, pp.109277.
- [26] Araya-Calvo, M., López-Gómez, I., Chamberlain-Simon, N., León-Salazar, J.L., Guillén-Girón, T., Corrales-Cordero, J.S. & Sánchez-Brenes, O., 2018. Evaluation of compressive and flexural properties of continuous fiber fabrication additive manufacturing technology. *Additive Manufacturing*, 22, pp.157-164.
- [27] Yang, C., Tian, X., Liu, T., Cao, Y. & Li, D., 2017. 3d printing for continuous fiber reinforced thermoplastic composites: Mechanism and performance. *Rapid Prototyping Journal*.
- [28] Astm 2014. Astm d3039/d3039m-08: Standard test method for tensile properties of polymer matrix composite materials. ASTM International.

[29] Astm 2017. Astm d790-17: Standard test methods for flexural properties of unreinforced and reinforced plastics and electrical insulating materials. ASTM International.

[30] Becker, W.T. & Shipley, R.J., 2002. *Asm handbook: Volume 11: Failure analysis and prevention*. ASM International.